

Damage Identification in Composite Panels—Methodologies and Visualisation

Richard Loendersloot, Inka Buethe, Pavlos Michaelides,
Maria Moix-Bonet and George Lampeas

Abstract A methodology for the identification of an impact damage using guided waves on a composite structure is implemented. Both numerical and experimental results are used, and a graphical user interface is developed to visualise the potentially damaged area. The latter allows, on top of detection, an assessment of the location and severity of the damage. The input can be experimentally based or calculated with the help of numerical models. Within this work, two numerical models are presented, based on stacked-shell finite element approach and on spectral element approach in time domain. The graphical interface allows the user to choose the most suitable approach from various damage identification methods using pitch-catch acousto-ultrasonics. The numerical models allow us to test a variety of damage locations with variable extents. The quality of the models is shown by a comparison of simulated and experimental data in time domain and respective damage indices. Finally, the visualisation allows to focus on specific areas, enhancing the analysis of multiple damages in a structure. The damage

R. Loendersloot (✉)

University of Twente, Engineering Technology, Dynamics Based Maintenance, P.O. Box 217, 7500 AE Enschede, The Netherlands
e-mail: r.loendersloot@utwente.nl

I. Buethe

Institute of Mechanics and Control Engineering—Mechatronics, University of Siegen, 57076 Siegen, Germany
e-mail: inka.buethe@uni-siegen.de

P. Michaelides

NASTECH—Novel Aerospace Technologies, Ancarano 64010, Italy

M. Moix-Bonet

Multifunctional Materials, Institute of Composite Structures and Adaptive Systems, German Aerospace Center, Lilienthalplatz 7, 38108 Braunschweig, Germany
e-mail: maria.moix-bonet@dlr.de

G. Lampeas

University of Patras, Laboratory of Technology and Strength of Materials, Department of Mechanical Engineering and Aeronautics, 26500 Rion, Patras, Greece

© Springer International Publishing Switzerland 2016

P.C. Wölcken and M. Papadopoulos (eds.), *Smart Intelligent Aircraft Structures (SARISTU)*, DOI 10.1007/978-3-319-22413-8_26

579

identification tool is a powerful tool in understanding the effects of various damage scenarios on the time response data and together with the numerical model provides a valuable input for model-assisted probability of detection (MAPOD).

Nomenclature

A_p	Ripple amplitude
A_{st}	Amplitude attenuation
D	Diameter
D	Damaged state (subscript)
DI	Damage index
E	Modulus of elasticity
F	Frequency
f	Filtered (subscript)
f_a	Actuation frequency
f_c	Cut-off frequency
G	Shear modulus
H	Thickness
H	Healthy state (subscript)
i, j, k	Index
$I(x, y)$	Damage intensity as function of spatial coordinates
L	Length
lpf	Low-pass filter (subscript)
N	Filter order or total number
N_p	Number of actuator–sensor paths
$R(x, y)$	Relative distance as function of spatial coordinates
$s(t)$	Time signal of piezoelectric transducer
$S(\omega)$	Frequency domain signal of piezoelectric transducer
T	Time
t_{layer}	Layer thickness
t_{PWAS}	Thickness of piezoelectric wafer active sensor
W	Width
x, y	Spatial coordinates
$X(\omega)$	Frequency domain function of low-pass filter
B	Scaling
N	Poisson ratio
P	Correlation coefficient
ρ_v	Volumetric density
ω	Angular frequency
A0	First asymmetric guided wave
AS	Application scenario
CFRP	Carbon fibre-reinforced plastic
GUI	Graphical user interface
IS	Integration scenario
MAPOD	Model-assisted probability of detection

PWAS	Piezoelectric wafer active sensor
S0	First symmetric guided wave
SEM	Spectral element method
SS-FEM	Stacked-shell finite element method

1 Introduction

The objective of application scenario 6 (AS06) of the SARISTU project is to develop a tool to assess an impact damage in a composite structure. The assessment relies on the use of integrated ultrasonic sensors, and the composite structures under investigation are representative for a door surrounding structure. The methods developed should be able to identify *barely visible impact damages*, effectively translated to delaminations with a minimum radius 20 ± 5 mm: all smaller delaminations are in principle considered to be too small to be detected reliably, but all larger delaminations are expected to be found as they pose a safety risk for the component. The accuracy in location is specified to be ± 10 mm.

The door surrounding representative composite structure is a quasi-isotropic, prepreg-based composite skin structure stiffened with Omega stringers that are cobonded to the structure. Within AS06, flat plates with and without stiffeners are investigated as well as curved plates with stiffeners. The full-scale door surrounding structure, as manufactured in the integration scenario (IS13), is also curved.

The tool has to have the functionality to support the inspection process and decision-making process regarding maintenance and repair of structures. A graphical interface is a prerequisite for this. The graphical user interface should allow the user to analyse data, choosing various options related to the type of analysis and region of interest, while not requesting in-depth knowledge on the algorithms implemented. It should also provide a clear output to be used in, for example (model-assisted) probability of detection—(MA)POD—analysis. Visualisation of the data and the potentially damaged area is an important element in the user interface.

The main principle of the damage assessment is that an acousto-ultrasonic signal is used to interrogate the structure. Typically, this implies a windowed wave packet containing a limited number (~ 3 – 10) of sine waves with a frequency in the order of 50–500 kHz. The signal is subsequently registered by a sensor positioned at some distance from the actuator. The way the signal is altered while travelling through the material forms the base of the damage assessment. The signal is also subjected to a number of environmental influences and noise. Signal processing techniques are applied to the raw data signals to reduce noise and eliminate crosstalk (the interference of signals of different channels, for example the actuation signal and the sensor signal channels).

Piezoelectric transducers are employed as actuators and sensors. Here, a network of transducers, referred to as a *workspace*, is considered, in which all transducers

can act as actuator and sensor. If one transducer is assigned as actuator, the others act as sensors. Each straight line from actuator to sensor is referred to as a *path*. A full coverage of paths for the area enclosed by the transducers is obtained by alternating the actuator. Note that each path provides information on the possible presence of damage close to the path, but only the combination of paths provides sufficient information to localise potentially damaged spot. This is partly caused by the reversibility assumption: it is assumed that switching the actuator and sensor for a path does not affect the resulting signal. Strictly taken, this assumption only holds for the pristine situation, since damage will introduce nonlinearities [1]. The assumption implies that the signal does not hold any information on the location of the possible damage on the path. For that reason, each path is only measured once, with each actuation frequency.

Damage assessment can be based on a single set of measurements (*unreferenced*) or on the comparison between measurements of the pristine condition and those of the current condition (*referenced*). The latter is used here, despite the fact that it may be difficult in practice to define the pristine state, as this state depends on environmental conditions: the pristine condition may not be representative if, for example, temperature, humidity or loading are different during the measurement of the current condition. However, the initial use of the tool is anticipated to be in the inspection phase, allowing to create a limited window of variability in the environmental condition: the aircraft will for example be on the ground, which provides some control on the environmental conditions.

Various algorithms are available to assess the presence of damage based on the comparison of pristine path signals and path signals from a structure potentially containing damage. The ability to identify damage depends on multiple factors, amongst which the frequency of actuation, the presence of stiffeners or transitions on a path and the location of the damage. An assessment of the performance of a large number of algorithms is therefore carried out. This assessment is briefly discussed in this paper.

Initially, flat panels without stiffeners are used to test the methods, both experimentally and numerically. This is motivated by the fact that the propagation of guided waves in a structure built from anisotropic layers is not well understood, in particular the response to the presence of damage and transitions such as a stiffener. Numerical models can assist in shedding light on the phenomena occurring when a wave travels through the material and encounters a flaw or transition in thickness or fibre orientation. Two numerical methods are implemented: the *spectral element model* (SEM) and a *stacked-shell finite element model* (SS-FEM).

2 Signal Processing and Damage Identification

The first task of the software developed for the acousto-ultrasonic damage identification is to load the data from a pristine and a potentially damaged case. This can either be data from experiments or from numerical models. In the first case, a

number of signal processing steps are required to prepare the data for the actual damage identification. This paper does not intend to discuss the origin of some of the distorting effects that are filtered during the signal processing phase, but merely presents the solution as it is implemented. There are three important signal processing steps:

1. Distortion of first few measurement points,
2. Zero offset and
3. Electro-magnetic crosstalk.

The first two are dealt with rather straightforwardly. The first few points (from experience, the default value is set to 5) are ignored by setting them to zero. Note that this corresponds to a time of 0.4 ns, given a typical sampling frequency of 12 MHz. The zero offset is corrected by subtracting the mean value (excluding the first few points that were already set to zero) from the signal.

The electro-magnetic crosstalk poses more challenges. Without going in further details, it can be stated that the length of the part of the sensor signal that is affected by the crosstalk is related to the actuation frequency and the number of cycles in a burst—be it not directly. A pragmatic approach would be to simply ignore the part of the signal that is affected by the crosstalk. However, in some cases, the real response of the sensor starts before the effect of the crosstalk has vanished.

To this end, a filter routine is implemented. It is assumed that the crosstalk signal mainly contains the actuation frequency. This is a reasonable, but not entirely correct assumption, as was shown by Moix-Bonet in a technical report issued in the SARISTU project [2]. The problem with using a more accurate representation of the actuation signal is that the number of cycles in the crosstalk signal does not correspond to the number of cycles in the actuation signal (6 against 5 cycles). Filtering only the actuation frequency will leave some high-frequency components behind, but these are small compared to the actual sensor signal. Evidently, the actuation frequency will also be present in the sensor signal, leading to a part of the actual sensor signal being unintendently filtered in case there is overlap between the crosstalk signal and the actual sensor signal. The overlap, if present, is small for the cases investigated, justifying the assumption that the filtering will not affect the damage identification. A flow chart of the filter routine is presented in Fig. 1.

The steps in the routine are visualised in Fig. 2. First, the raw signal (Fig. 2a) is loaded, after which a low-pass filter is applied with a cut-off frequency f_c of (by default) 150 % of the actuation frequency f_a (Fig. 2b). The software allows us to use different models for the low-pass filter—essentially, those offered by MATLAB. The filtered signal is shown in Fig. 2c, which is subtracted from the original signal (Fig. 2a), yielding the filtered signal in Fig. 2d. The experimental data from a flat panel with stiffeners are used for this illustration. An actuation frequency of 80 kHz was used, leading to a cut-off frequency of 120 kHz. The maximum ripple in the passband ($f < f_c$) is set to 1 dB, while the attenuation of 80 dB is used for the stop band ($f > f_c$).

Once the raw data are processed, the damage identification algorithms can be applied. The approach followed corresponds with the signal correlation analysis

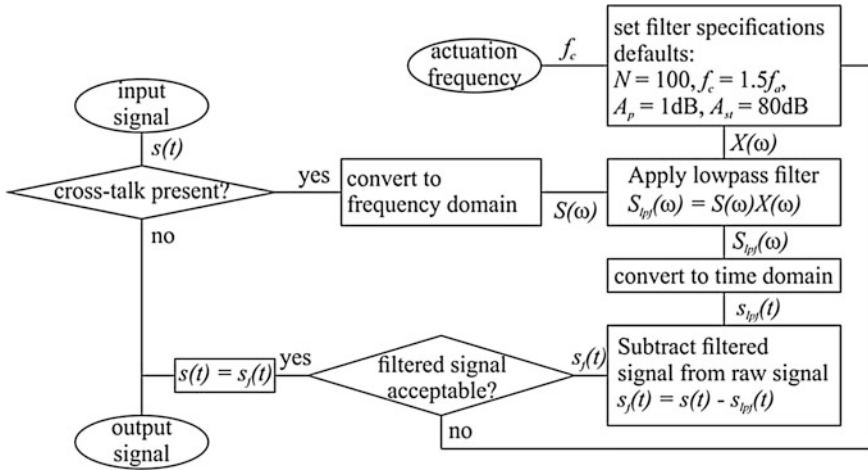


Fig. 1 Flow chart of the electro-mechanical crosstalk filter

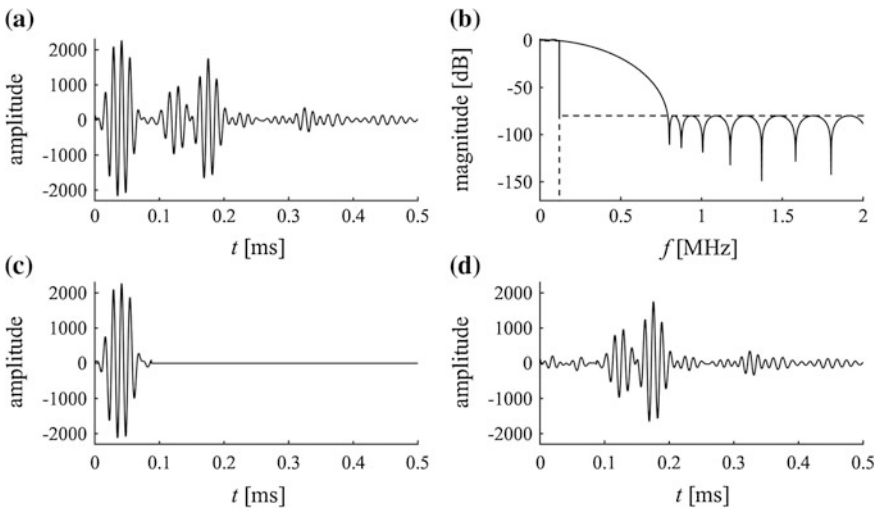


Fig. 2 Graphical overview of the crosstalk routine. Raw signal from experimental data from a flat test panel with Omega stringers, actuation frequency 80 kHz, cut-off frequency 120 kHz, passband ripple 1 dB and stop band amplitude attenuation 80 dB. **a** The raw signal; **b** the low-pass filter; **c** the low-pass filtered signal; and **d** the raw signal minus the low-pass filtered signal

technique as described by Su and Ye [1]. First, a grid is defined, overlaying the panel. The damage intensity $I(x,y)$ at each grid point (x,y) is calculated, by assuming a certain area of influence of the actuator–sensor paths. The damage intensity is defined as follows:

$$I(x, y) = \sum_{k=1}^{N_p} (1 - \rho_k) \left(\frac{\beta - R(x, y)}{\beta - 1} \right) \tag{1}$$

where ρ_k being the correlation coefficient of the k th actuator–sensor path, N_p the number of paths, β the scaling factor determining the area of influence and $R(x, y)$ defined as:

$$R(x, y) = \begin{cases} \frac{\sqrt{(x-x_i)^2+(y-y_i)^2} + \sqrt{(x-x_j)^2+(y-y_j)^2}}{\sqrt{(x_i-x_j)^2+(y_i-y_j)^2}} & \text{for } R(x, y) < \beta \\ \beta & \text{for } R(x, y) \geq \beta \end{cases} \tag{2}$$

where (x_i, y_i) and (x_j, y_j) indicate the locations of transducer i and j , respectively. Typically, β is equal to 1.05. Su and Ye [1] use the correlation coefficient as an indicator of damage. The correlation coefficient equals one if there is no damage and is lower than one if there is damage (as the correlation between the signals will be less).

The correlation function is not the only possible indicator of damage: there are many methods to calculate a damage index (DI). Fourteen methods are implemented and tested on their performance [3] next to the method based on the correlation coefficient. The damage indices are based on signal’s intensity, time of an event (e.g. time of flight), frequency domain expressions, signal energy, etc. In every method, attributes of baseline (healthy) and currently acquired (unknown health state) signals are compared to identify potential change in the structural characteristics, which in turn would be an indication of damage. The performance depends on the type of damage (i.e. how the signal is affected) and on the actuation frequency. It is therefore difficult, if not impossible, to formulate definite conclusions on the performance.

The methodologies implemented, along with their mathematical formulas, are presented in Table 1. This allows the user to mutually compare methods and select the best performing method for the case under investigation. An issue to address is that the damage index that is calculated in most methods gives a value of zero if no damage is present and tends to infinity (theoretically, in practice a large number) if there is damage. The following relation applies between the value of the correlation coefficient and the damage index:

$$\rho_k = \frac{1}{DI + 1} \tag{3}$$

The only exceptions are the signal amplitude peak ratio (SAPR) method and the ratio of covariance matrix eigenvalues (RCME) method. In case of the SAPR method, the damage index equals 1, rather than 0 in case of no damage, but also tends to infinity in case of damage: the ‘+1’ in the denominator of Eq. 3 is dropped. The RCME method gives a value between 1 and 0 for the healthy and damaged

Table 1 Damage identification algorithms implemented in the software

	Method name	Abbr.	Mathematical formula
1	Correlation coefficient	CC	$\rho = \frac{\sum_{i=1}^N S_{H,i} S_{D,i} - \sum_{i=1}^N S_{H,i} \sum_{i=1}^N S_{D,i}}{\sqrt{\sum_{i=1}^N S_{H,i}^2 - (\sum_{i=1}^N S_{H,i})^2} \cdot \sqrt{\sum_{i=1}^N S_{D,i}^2 - (\sum_{i=1}^N S_{D,i})^2}}$
2	Signal amplitude peak ratio	SAPR	$DI = \frac{\max[S_H]}{\max[S_D]}$
3	Signal amplitude peak squared percentage differences	SAPS	$DI = \left(\frac{\max[S_H] - \max[S_D]}{\max[S_H]} \right)^2$
4	Signal amplitude hilbert transform maximum	SAHM	$DI = \left \frac{\max[H[S_H]] - \max[H[S_D]]}{\max[H[S_H]]} \right $
5	Signal sum of squared differences	SSSD	$DI = \frac{\sum (S_H - S_D)^2}{\sum S_H^2}$
6	Welch-based power spectral density	WPSD	$DI = \frac{\left \int_0^{2/f_{ex}} PW[S_D] df - \int_0^{2/f_{ex}} PW[S_H] df \right }{\int_0^{2/f_{ex}} PW[S_H] df}$
7	Welch-based transfer function	WTF	$DI = \frac{\left \int_0^{2/f_{ex}} TF[S_D] df - \int_0^{2/f_{ex}} TF[S_H] df \right }{\int_0^{2/f_{ex}} TF[S_H] df}$
8	Parametric (AR-based) power spectral density	ARPSD	$DI = \frac{\left \int_0^{2/f_{ex}} PAR[S_D] df - \int_0^{2/f_{ex}} PAR[S_H] df \right }{\int_0^{2/f_{ex}} PAR[S_H] df}$
9	Parametric (AR-based) resonance frequency differences	ARRFD	$DI = \frac{\left f_{peak}^H - f_{peak}^D \right }{f_{peak}^H}$ $f_{peak}^{H,D} = \underset{f}{\operatorname{argmax}} [PAR[S_{H,D}(f)]]$
10	Parametric (AR-based) chi-squared statistic	ARCS	$DI = \delta P^T \cdot \delta C \cdot \delta P$ $\delta P = P_H - P_D; \delta C = C_H + C_D$
11	Cross-correlation-based TOF percentage difference	CCTOF	$DI = \frac{ t_{max} CC^H - t_{max} CC^D }{t_{max} CC^H}$ $t_{maxCC}^{H,D} = \underset{t}{\operatorname{argmax}} [CC_{H,D}(t)]$
12	Cross-correlation maximum percentage difference	CCMPD	$DI = \frac{ \max[CC_H] - \max[CC_D] }{\max[CC_H]}$
13	Hilbert transform-based TOF percentage difference	HTOF	$DI = \frac{ t_{maxH}^H - t_{maxH}^D }{t_{maxH}^H}$ $t_{maxCC}^{H,D} = \underset{t}{\operatorname{argmax}} [H[S_{H,D}(t)]]$
14	Discrete wavelet transform approximation coefficient-based DI	DWTC	$DI = \frac{\sum (DWT[S_H] - DWT[S_D])^2}{\sum DWT[S_H]^2}$
15	Ratio of covariance matrix eigenvalues	RCME	$\rho = 1 - \frac{\lambda_2}{\lambda_1}$

state, respectively, like the correlation coefficient. Using Eq. 3 allows to use any damage indicator in combination with the damage intensity $I(x,y)$ as defined in Eq. 1.

3 Software with Graphical User Interface

The routines to convert the raw data signals to a coloured contour plot indicating possible damage locations are embedded in a software package with a graphical user interface (GUI). The user can quickly analyse a set of measured responses, without having to be an expert in the signal processing and damage identification algorithms. It is however also possible to tune many of the variables, allowing a more experienced user to perform a more detailed analysis of the data.

Both experimental and numerical data can be analysed with the GUI. It is therefore, for example, possible to run a series of numerical analysis to investigate the effect of specific damage characteristics on the capability of the damage identification process. A better understanding of these effects will enhance the interpretation of experimental results (Sect. 6). An example of the analysis of data from numerical models is presented in Sect. 5.

The GUI is structured in three sections: a section with buttons to toggle between the different user control panels; a section for the user control panels; and a section for graphical representations. There are five different user control panels, overlaying each other and allowing the user to control the operations applied to the data. These panels are as follows:

1. The file load panel,
2. The preprocessor panel,
3. The algorithms panel,
4. The data visualisation panel, and
5. The export panel.

Some additional functionality is embedded in the part with the graphical representation, as well as in the part of the menu block. Note that one can only proceed to the other sections of the software once a complete data set is loaded.

3.1 File Load

The software is developed to handle different types of input. Data that can be loaded are experimental data from the ScanGenie system as used by the DLR and especially Airbus, experimental data from measurements from the University of Siegen and numerical data from the models from the University of Siegen and the University of Patras. The format of the data is different. Hence, the user first needs to select the type of data. A distinction is made between geometrical data and

signals from the transducers. Although currently not implemented, an additional functionality is scheduled to be implemented to specify the geometrical properties (partly) manually.

The signals from the transducers are restructured to obtain a memory efficient and logical structure. The memory efficiency is significantly higher than the default structure of the ScanGenie MATLAB export; this contains a fair amount of redundancy, since the actuator signal is stored for each path, also if the sensor signal from another path is obtained from the very same actuator signal. In general, a number of transducer act as sensor each time a transducer is acting as actuator. All sensor signals of a single actuation cycle are saved together with the actuator signal of that cycle. This avoids redundancy and in the end allows the user to load multiple cases at once, without running into memory-related errors or slow functioning of the computer.



Fig. 3 File load panel. The file containing the geometric information is selected in the *top part*; once loaded, the *lower part* of the panel becomes active and the signal data files can be specified and loaded

The panel in the software with all the options for loading the geometry and data files is shown in Fig. 3. Note that a geometry file must first be loaded before it is possible to load data files. Moreover, it is possible to analyse data files without a reference or baseline file, although no damage identification algorithms are implemented for this case, leaving only a limited number of functions available in the visualisation section. Finally, one can also choose to load a configuration. A file saved from a previous analysis is then loaded. It can contain anything from just the geometry to the damage identification data. The ‘save’ button allows to save the data that is in the program at that moment, creating a configuration file. This allows the user to create a restart point at any time wanted.

3.2 *Preprocessor*

The signal processing steps described in Section 2 of this paper can be activated in this part of the software (see Fig. 4). The user can decide to skip these, as, for example, the numerical data do not show electro-magnetic crosstalk. It is also possible to change settings of the signal processing steps, although it is recommended to follow the default settings if one is not familiar with the signal processing concepts.

The crosstalk filter takes the largest part of the preprocessor panel. Most graphical elements are related to settings of the filter and will not further be addressed here. It is however important to note that the filtering is first applied to a copy of the data and shown to the user in the graphical visualisation panel on the right-hand side of the GUI. Initially, only a limited set of signals is shown, due to the large amount of signals. The user can select other signals to be shown by selecting the signals in the list box next to the main graphical area. The filter is only applied upon acceptance by the user; the original data are overwritten by the filtered data, and the temporary data are deleted.

Finally, the grid for the damage plot has to be created. The default is a (nearly) square grid, with a density based on the dimensions of the workspace; the number of elements must be an integer number, and therefore, the edge lengths are set as close as possible to a square grid by default. The ratio of the grid dimensions can also be unconstrained, resulting in a rectangular grid, and the grid can also be based on edge size rather than on a number of elements in each direction. Again, the edge lengths are adjusted to obtain the nearest integer number for the number of elements along the domain edge.

3.3 *Algorithm*

Once the data have passed through the necessary signal processing steps, a damage identification method can be selected. The pop-up menu in this panel (see Fig. 5)

The image shows a software interface titled "Preprocessor" with several sections:

- Correction first values:** A text input field containing "5", with "Apply" and "Save" buttons.
- Correction zero-offset:** A text input field containing "0", with "Apply" and "Save" buttons.
- Crosstalk filter - Lowpass filter:**
 - A dropdown menu showing "N,Fp,Ap,Ast" with "Apply" and "Accept" buttons.
 - Parameters: Order (100), Denom (50), Num (50).
 - Parameters: Fp (1.5), Fst (2), F3db (2.5), Fc (2.5).
 - Parameters: Ap (1), Ast (80).
 - A dropdown menu showing "250000" and a checked "Freq. dependent" checkbox.
 - "Save" button.
- Geometry:**
 - A dropdown menu showing "Map".
 - A checked "Constrain pixel ratio" checkbox.
 - Two text input fields, both containing "36".
 - A dropdown menu showing "Number".
 - "Create" and "Save" buttons.

Fig. 4 Preprocessor panel. The signal processing steps are defined in the three sections on the *top* of the panel, whereas the creation of the grid for mapping the damage intensity is controlled in the *bottom section* of the panel

provides the possibility to select one of the algorithms listed in Table 1. It is not possible yet to select more than one damage identification algorithm, although this is foreseen to be implemented in future versions. Moreover, it is not yet possible to change any of the parameters of the algorithms. Although not all algorithms have variables that can be set, it may be of interest to fine tune specific algorithms.

The damage identification algorithms are applied to all combinations of reference and current data sets. If multiple reference data sets are used, the difference between these data sets can also be analysed, which gives an indication of the

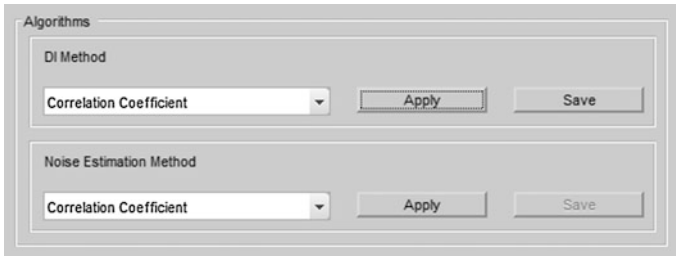


Fig. 5 Algorithm panel. The algorithms to be used for the damage identification and the noise estimation (if multiple reference files are loaded) can be selected individually

scatter of the measurements. The same algorithms are used for this noise estimation as are used for the damage identification, and again, all possible combinations of data sets are analysed.

3.4 Visualisation

Various aspects can be shown in the graphical representation area. The visualisation panel (Fig. 6) allows the user to control what is shown. First of all, the geometry can be shown. This means the geometry of the entire panel, but also that of (one of) the workspace(s). If a workspace is selected, the paths can be added to the plot.

Secondly, the raw data can be plot. The term ‘raw’ here refers to the time data of the transducers that are stored, after the signal processing if applied. The actuator and sensor signals are separated as are the reference and current state data, resulting in a set of four graphs. The raw data plot is the only plot that can be made if no reference data are loaded. In that case, only two graphs are shown.

The largest subpanel is the damage surface plot section. The damage intensity $I(x,y)$ is plotted as a coloured surface plot, using Eqs. 1 and 2. The colour indicates the intensity, where blue refers to a low intensity (no damage) and yellow to a high likelihood of damage. The absolute values of the damage intensities are given in the colour bar that is either positioned below or aside the main plot. It is possible to show the intensity for specific actuation frequencies, if multiple actuation frequencies are used. Note that in general only a single actuation frequency is used per actuator, such that an incomplete path coverage is obtained if not all actuation frequencies are included. Multiple damage indices per path are available if multiple actuation frequencies per actuator are used; the user can choose to plot the maximum, mean or minimum intensity in that case.

The intensity gives an indication of possible damage locations. However, it is up to the user to set a threshold, as the absolute value of the damage intensity depends on many variables, such as the type and location of the damage or the presence of other damages, and no physical interpretation is available to set a general threshold. A slider can be used to set the threshold. If a threshold is set, dynamic contour lines



Fig. 6 Visualisation panel. This panel permits the user to control the graphical output displayed on the right-hand side of the GUI (not visible here)

are plot, indicating the border between the intensities below and above the threshold. The contour lines are updated each time the threshold is changed. A potentially damaged area can be selected by choosing a proper threshold value. Square markers are added as well, indicating peaks in the damage intensity. A peak is defined as a damage intensity value that is higher than the damage intensity of all its surrounding points and higher than a preset (hardcoded) threshold. Once the threshold is set, an area enclosed by a contour can be selected. The damage index of the area is subsequently stored. The user can now either focus further on the area

enclosed in the contour, by isolating it, or focus on other areas by excluding this. The colour scaling of the intensity is updated after isolation or exclusion of the area enclosed by the contour. Thus, in case of the latter, secondary potentially damaged areas can more easily be identified: this procedure offers unique possibilities for assessing multiple damages in the structure.

3.5 Export

The damage intensity indicates *possible* locations for the damage: to investigate the likelihood that it concerns a real damage, the data need to be exported and subsequently imported in a probability of detection analysis. The data to export are controlled in the export panel (Fig. 7). Prior to be allowed to enter this section, at

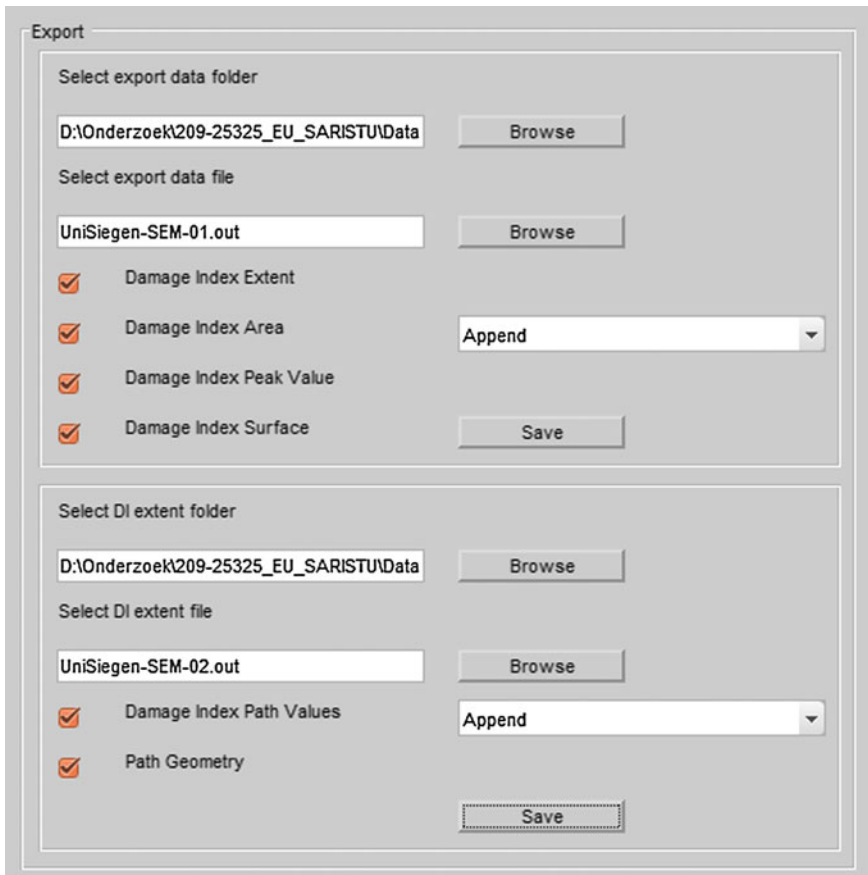


Fig. 7 Export panel. Two different output files, both in ASCII format, can be exported. The content of the files can be adapted by (de)activating the checkboxes

least one damaged area must be identified, by setting a threshold for the damage intensity and selecting an area enclosed by a contour. Two different export files, both in ASCII format, can be exported:

1. Data file containing information on the damage intensity in the contour(s) selected and
2. Data file containing the damage indices for each path.

The files start with a header providing information on the data files used, the date the file was created and the dates it was appended (if). The damage extent file then contains by default four elements for each contour that is exported:

1. The damage intensity integrated over the area enclosed by the contour,
2. The area enclosed by the contour,
3. The coordinates of the peaks in the contour and their values, and
4. The centre coordinates of all grid elements in the contour and their damage intensity value

The user can chose to deselect each of these items to exclude them from being exported. The damage path file contains per path in a workspace the following information:

1. The transducer number of the actuator,
2. The transducer number of the sensor,
3. The actuation frequency,
4. The damage index of the path,
5. The x -coordinate of the actuator,
6. The y -coordinate of the actuator,
7. The x -coordinate of the sensor,
8. The y -coordinate of the sensor and
9. The length of the path

Again, the user can control which of these items are included in the export file.

3.6 *Graphs*

The data visualisation panel covers approximately 50 % of the GUI. It mainly contains space to display graphs, either from the geometry, the signals or the damage intensity. Some additional functionality is added to facilitate the export of graphs. The buttons ‘undock’ and ‘redock’ are used to transfer the data to a separate figure window and vice versa. The user can manipulate the graphical material in the separate figure, using the built-in MATLAB functionalities. The graphical visualisation panel is shown in Fig. 12.

4 Numerical Modelling

Developing a finite element (FE) model can contribute to the understanding of the scattering phenomena of Lamb waves upon encountering structural damage. Standard FE model has a number of limitations that should be taken into account:

- A fine FE mesh, comprising at least 10 or even more nodes per Lamb wavelength, is a prerequisite to deliver good spatial precision;
- A laminate may have to be divided into sublaminates in thickness, to properly represent interlaminar damage and damage into the individual laminas;
- The time step for dynamic calculation should be less than the ratio of the minimum distance of any two adjoining nodes to the maximum wave velocity (often the velocity of the S0 mode).

Two solutions to overcome these limitations are presented in this paper. The first method is the spectral element method (SEM), whereas the second relies on a stacked-shell FE model.

4.1 SEM

The spectral element method combines the advantages of global pseudospectral methods with the flexibility of finite element methods. One of the first use-cases can be found at [4], dealing with fluid dynamics. The use of the spectral element method in time domain for structural health monitoring in general is described in [5]. The SEM model used in this work is described in detail in [6]. The SEM model uses a flat shell spectral element, based on first-order plate theory (first-order shear deformation theory). As the structure is modelled with one element over the thickness for undamaged parts, the number of degrees of freedom is comparably small. The nodes for these elements are not distributed evenly, but follow the roots of a Gauss–Lobatto–Legendre polynomial. Their irregular distribution combined with the use of Lagrange interpolation polynomials as shape functions makes it possible to use less elements than necessary for traditional low-order FEM. In particular for higher frequencies and bigger structures, this is an advantage. Moreover, a band-like structure of system matrices (like mass matrix) enables a reduction of computational costs in time domain. Nevertheless to introduce delamination, the one element over the thickness has to be divided into two new elements, each comprising of multiple layers of the composite material; if a delamination is modelled between layer k and $k + 1$, then the bottom element contains layer 1 to k and the top element layers $k + 1$ to N , where N is the total number of layers. Note that this division causes more system matrix elements to differ from zero. The calculation of contact forces prohibits penetration of the two elements above and below the delamination. More information about the delamination introduction can be found in [7]. For the implementation of SEM, the

plate-like character has to be ensured. For this, the relation of size of the damage and plate thickness is important.

4.2 Stacked-Shell FEM

The three basic requirements mentioned above usually result in high demands in terms of computational cost, particularly for large composite structures. To balance the need for precision and computational efficiency, the ‘stacked-shell’ or ‘layered shell’ approach under the finite element method (SS-FEM) is investigated for the Lamb wave simulation. The explicit FE code LS-DYNA is used for this purpose. In the stacked-shell approach, the composite laminates are represented by a discrete number of sublaminates modelled as shell elements, which can be tied together with solid cohesive elements or contact interface elements with cohesive zone properties. These interfaces have the capability to behave as matrix interlayers which connect the plies and are capable to fail during the simulation when appropriate conditions are met, either by introducing a cohesive law in the interface, or by setting appropriate interface strength limits. A schematic of the stacked-shell approach is given in Fig. 8. It should be noted that the number of layers in the SS-FEM model does not need to correspond to the number lamina in the composite, although in the model implemented here, each lamina is represented by a shell layer.

The stacked-shell approach is capable of representing accurately the out-of-plane behaviour of laminated structures, while maintaining the higher computational efficiency and simplicity of conventional shell approaches. The main advantage comes from the disconnection of the mesh discretization requirements of the in-plane and the through-thickness directions of the structure; the mesh density of

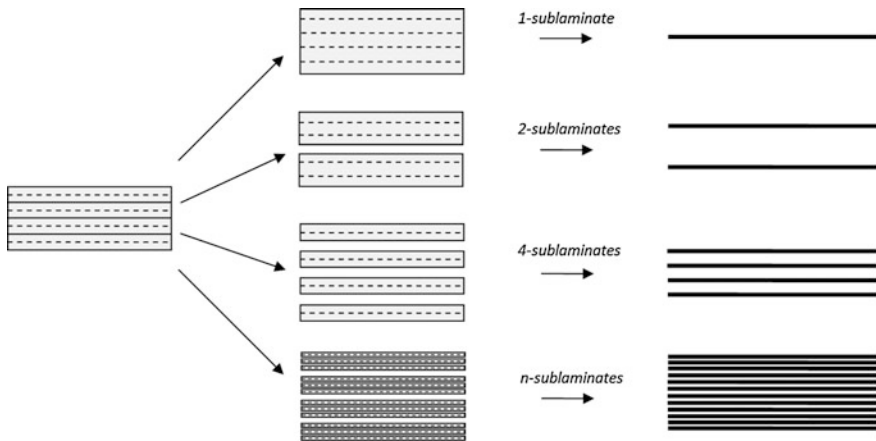


Fig. 8 Schematic of the stacked-shell approach. A 4-layer laminate is modelled by stacking 1-, 2-, 4- and n -sublaminates

the shell elements is independent of the through-thickness mesh density, whereas the latter normally dictates a significantly more dense mesh than the in-plane requirements demand. Furthermore, using the layered shell approach, an intrinsic delamination capability is introduced, i.e. delaminated areas can be easily and properly represented.

5 Use-Cases

Within the SARISTU project, a plate-like exemplary structure was used for experimental investigations, which can be compared to numerical simulations. This structure exhibits 11 layers of CFRP made from M21 matrix with T800S fibres. The properties of a layer of unidirectional composite material are listed in Table 2, the dimensions of the test panel and the piezoelectric transducers (PWAS—piezoelectric wafer active sensors), including their position in Table 3, whereas a schematic of the plate is presented in Fig. 9. The transducers are cobonded on the plate, making a shortening of the critical path on the production line possible. The actuator is excited by a five-cycle sinusoidal tone bursts, modulated utilising a Hanning window. Central frequency of 120 kHz (SS-FEM) and 250 kHz (SEM) is used.

5.1 Definition of the Test Cases

Various damage scenarios were implemented in the numerical models to test the damage identification algorithms in the software, as well as the capabilities of the

Table 2 Material properties of the CFRP [11 layers, (45, 0, -45, 90, 0, 90, 0, 90, -45, 0, 45), M21 matrix with T800 fibres]

E_x (GPa)	$E_y = E_z$ (GPa)	$G_{xy} = G_{xz}$ (GPa)	G_{yz} (GPa)	$\nu_{xy} = \nu_{xz}$ []	ν_{yz} []	ρ_v [$\text{kg}\cdot\text{m}^{-3}$]
157	8.5	4.2	2.2	0.35	0.53	1580

Table 3 Dimensions. Panel and the transducers including their location

	Symbol	Unit	Value			
Length	L	mm	500			
Width	W	mm	500			
Thickness	H	mm	2.024			
Layer thickness	t_{layer}	mm	0,184			
PWAS transducer	d	mm	6.35			
	t_{PWAS}	mm	0.25			
	x	mm	100	400		
	y	mm	100	200	300	400

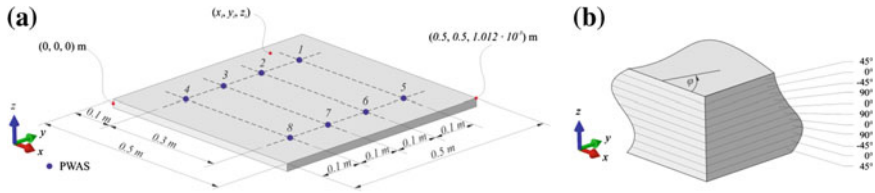


Fig. 9 Set-up of the SARISTU plate-like structure. Test structure for software, experiment and numerical simulations; **a** geometry with its dimensions and locations of the transducers; **b** the lay-up with orientation of the different layers

Table 4 Damage scenarios implemented in the numerical models

Scenario	Model	Shape	Dimensions	Location	Layer
1	SEM + experiment	Elliptical	$d_1 = 28 \text{ mm}$, $d_2 = 19 \text{ mm}$, $\theta = 45^\circ$	$(x,y) = (0.25,0.2)$	9–10
2	SS-FEM	Round	$d = 10 \text{ mm}$	$(x,y) = (0.25,0.4)$	1–2
3	SS-FEM	Round	$d = 10 \text{ mm}$	$(x,y) = (0.25,0.4)$	1–5
4	SS-FEM	Round	$d = 30 \text{ mm}$	$(x,y) = (0.25,0.4)$	10–11
5	SS-FEM	Round	$d = 30 \text{ mm}$	$(x,y) = (0.25,0.4)$	7–11

graphical representation of the damage offered by the software. The damage scenario of the SEM analysis is based on the experimentally introduced damage and differs from the damage scenarios in the SS-FEM model. The details are given in Table 4. Note that the composite layers are numbered from top to bottom.

5.2 Results of SEM Model

To validate the SEM model, measurements of the undamaged structure are compared with results from the SEM. An exemplary timeline is shown in Fig. 10. After a path independent scaling for all transducers, the wave packages of the different modes can be represented properly. To compare the results of the damaged structure, the software, described in Sect. 4, was used. The correlation coefficient has been exported for all paths. The path between PWAS 6 and PWAS 4 is directly crossing the damage zone, while all other paths starting at actuator 6 are not. As it can be seen in Fig. 11, the agreement between SEM simulation and experiment is fairly good.

The usage of SEM simulation data with the developed software is possible very easily. With its help, a damage localisation can be realised. As the simulation does not include noise, even from data of a single frequency, the localisation results are excellent. The output of the software is shown in Fig. 12. The red contour line is set by the user by increasing the threshold up to the desired level. It corresponds to the damage implemented in the numerical model, as defined in Table 4.

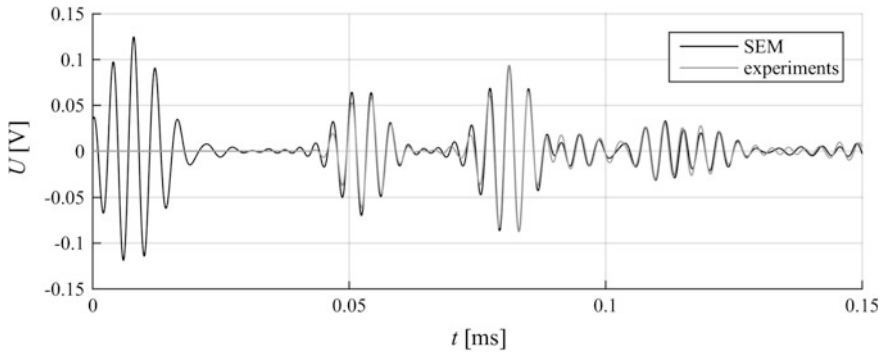


Fig. 10 Exemplary timeline to compare experimental and numerical SEM results. The different modes and their amplitudes can be simulated properly. An adaptation of the signal amplitude is necessary. This correction factor is the same for all sensing transducers

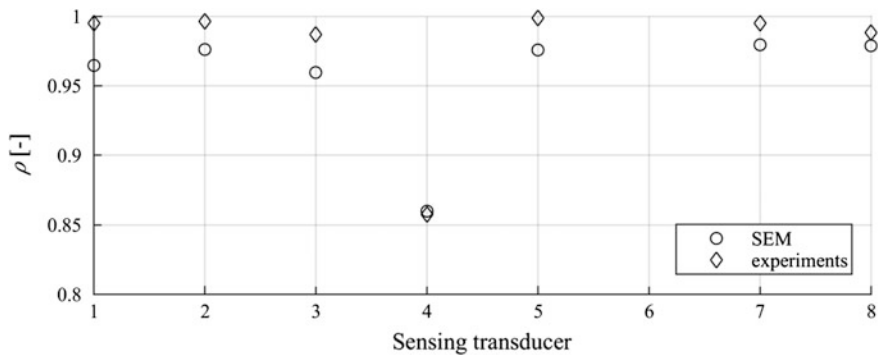


Fig. 11 Comparison of damage indices for SEM simulation and experiment. While for paths, which are not directly crossing the delamination, the experimental data results in slightly lower correlation coefficient, for the direct path, simulation and experimental results show an excellent agreement

5.3 Results of the SS-FEM Model

An indicative comparison of the numerical and experimental time response results for the undamaged case, in which transducer 1 is the actuator and transducers 2–8 are sensors, is presented in Fig. 13. The presented results refer to calculated strain values at the position of sensor 3.

From the indicative comparison of Fig. 13, it arises that the methodology seems effective for the simulation of Lamb wave propagation: a qualitative correspondence of the results is obtained. However, the need for further development and optimisation of the simulation parameters is obvious as well. Improvements are

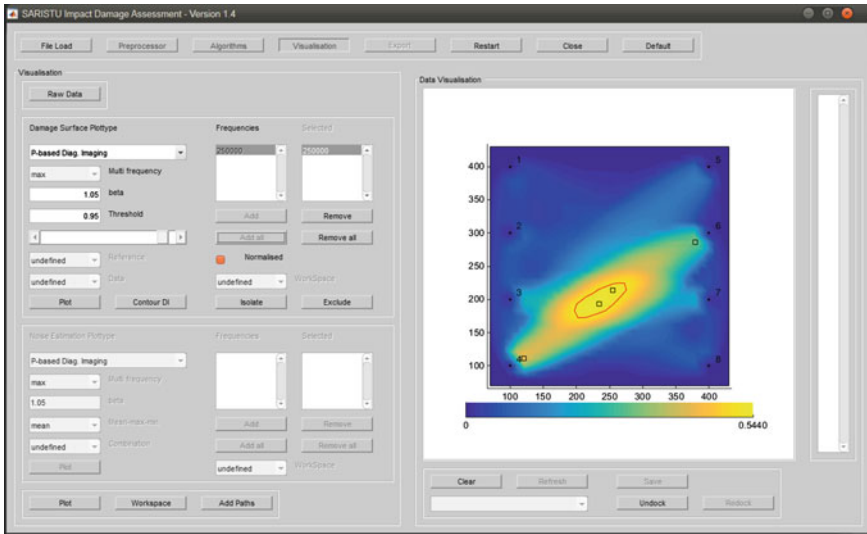


Fig. 12 Output of the software for damage localisation. Using the SEM simulations as input, the software detects the damage with the help of the correlation coefficient and localises it with path-based methods. The *red contour line* is set by the user by increasing the threshold level to the desired level. The *square markers* indicate maxima in the damage intensity

foreseen to be achieved by means of mesh convergence studies for the in-plane mesh density and an optimisation of the number of sublaminates. Finally, a calibration of the simulation parameters, to match the real properties of the panel from which the experimental results are obtained, will further diminish the differences between the simulation and the experimental results.

The time response results of transducer 5 for the various damage cases investigated are compared to the response of that transducer for a pristine structure. The results are depicted in Fig. 14. The ultrasonic wave generated by the actuator (here transducer 1) crosses the damage, that is located in the middle of the path from transducer 1–5.

It can be observed, from Fig. 14, that the signal from the damaged panels is slightly reduced compared to the signal of the pristine panel. The amplitude reduction is marginal; the only visible difference is from the case of a damage with a 30 mm diameter located at the top of the laminate (the side of the transducers).

5.4 Discussion of the Numerical Models

A first analysis of the two numerical models indicates that a higher accuracy is obtained using the SEM model. The SS-FEM model is less accurate when

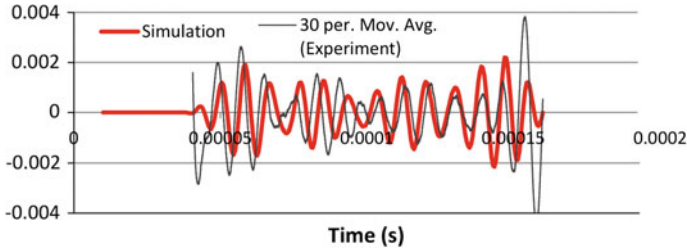


Fig. 13 Comparison of numerical and experimental time response. Results of transducer 3 for the undamaged flat panel case

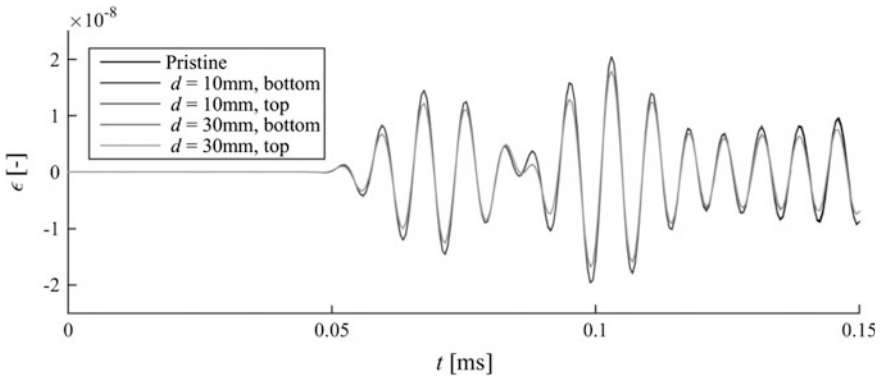


Fig. 14 Comparison of numerical responses between undamaged and damaged flat panels for transducer 5. The damage is located in the middle of the path from transducer 1 (which acts as the actuator) to 5. Only the response of the case with the 30 mm delamination located at the top differs visually from the pristine response

compared to the experimental results. However, the SEM model only allows for the modelling of a single-layer delamination in the material, whereas a complex, but far more realistic, multilayer delamination can be modelled in the SS-FEM model. This by itself offers valuable opportunities to enhance the damage identification, since it is to be expected that the response to a delamination with a certain area, located between two layers close to the surface, will cause a similar damage intensity, but different response when compared to a delamination spanning multiple layers, but with a smaller area. The SS-FEM indicates a difference in the response depending on the location of the damage, but unfortunately, the results show that the difference lies in being detected or not. However, it must be noted that the SS-FEM results are based on a limited set of paths, with only transducer 1 acting as an actuator. At this point, it is difficult to compare the numerical models in more detail, since a different type of damage is implemented (see Table 4).

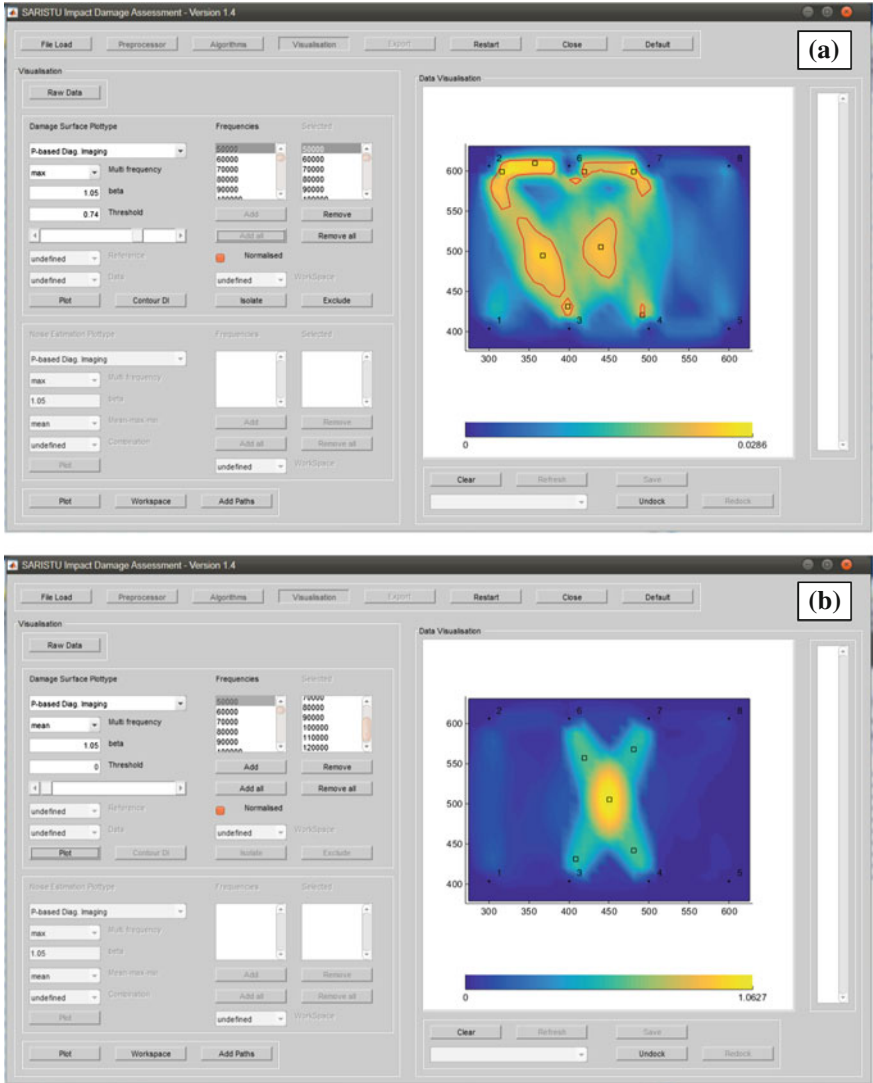


Fig. 15 Output of the software damage identification. Experimental data of a flat panel with Omega stringers is used. Actuation frequencies from 50 to 300 kHz are used. The *red contours* indicate potentially damaged area. The damage is located in the centre of the image. **a** Using all actuation frequencies and the maximum value of the correlation coefficient for each actuator–sensor path; **b** using a subset of the actuation frequencies and the mean value of the correlation coefficient for each path

5.5 Results of Experimental Data

The software is also tested on experimental results in order to assess the influence of environmental conditions on the capability of the damage identification algorithms. The environmental conditions are mainly limited to the higher level of noise that is observed in experiments compared to numerical models, since the experiments were performed in a relatively well-controlled laboratory environment. Instead of using a single actuation frequency, multiple actuation frequencies were used, ranging from 50 to 300 kHz. The resulting damage intensity plot, based on the correlation coefficient damage identification algorithm, is shown in Fig. 15. The difference between using all frequencies or a subset (all frequencies up to 120 kHz) and using the maximum or the mean of the correlation coefficient of each actuator–sensor path is highlighted clearly by the two damage intensity plots in Fig. 15: the top figure shows a lot of disturbance making it difficult to unambiguously identify the location of the damage, whereas the lower figure clearly indicates the location of the damage. The choices of the actuation frequencies, the damage identification method and other settings are clearly relevant, but sometime hard to make beforehand. The software allows to analyse the effect of these choices in a quick and convenient manner.

6 Conclusion

It has been shown that the software for the damage identification discussed in this paper offers a convenient manner of analysis of data from monitoring tests, based on a network of piezoelectric transducers. The software can handle both numerical and experimental data, making it suitable to be used in both the design phase of a monitoring system as well as in the use phase. The user can analyse the data without an in-depth knowledge on the signal processing algorithms that are implemented, but can at the same time adjust all kind of settings, making the software a powerful tool both for a quick scan of measured data and for a more elaborate investigation by an experienced user (in the field of signal processing).

The numerical models show different results: the SEM model is more accurate compared to the SS-FEM model in terms of correspondence to the experimental results. The SS-FEM promises a more detailed representation of the damage, by allowing the damage to span different layers. The accuracy of the SS-FEM method is however still not at the desired level.

Acknowledgments The research leading to these results has received funding from the European Union's Seventh Framework Programme for research, technological development and demonstration under Grant Agreement No 284562.

References

1. Su Z, Ye L (2009) Identification of damage using lamb waves—from fundamentals to applications. Lecture notes in applied and computational mechanics, vol 48. Springer, Berlin
2. Moix-Bonet M (2012) Guidelines for the signal processing algorithm. Technical Report of SARISTU project
3. Michaelides PG (2013) Pitch catch algorithms preliminary analysis. Technical Report of SARISTU project
4. Patera AT (1984) A spectral element method for fluid dynamics—laminar flow in a channel expansion. *J Comput Phys* 54:468–488
5. Ostachowicz W, Kudela P, Krawczuk M, Zak A (2012) Guided waves in structures for SHM—the time-domain spectral element method. Wiley, New York
6. Schulte RT (2010) Modellierung und Simulation von wellenbasierten Structural Health Monitoring – Systemen mit der Spektral-Elemente Methode. PhD thesis, University of Siegen (2010)
7. Jung H, Schulte RT, Fritzen, C-P (2011) Interaction of elastic waves with delaminations in CFRP structures: a numerical study using the spectral element method. In: Chang F-K (eds) Structural health monitoring, 8th international workshop on structural health monitoring, Stanford, September 2011, pp 2576–2583